A Partial Power Processing Structure Embedding Renewable Energy Source and Energy Storage Element for Islanded DC Microgrid

Nie Hou, *Member, IEEE*, Li Ding, *Member, IEEE*, Pasan Gunawardena, *Graduate Student Member, IEEE*, TianHong Wang, *Member, IEEE*, Yue Zhang, *Member, IEEE*, and Yun Wei Li, *Fellow, IEEE*

***Abstract*—In the past ten years, because of less power transferred loss, the partial power processing (PPP) converter systems are extensively studied for embedding the renewable energy source (RES) into the strong grid system. Moreover, by combining the energy storage system (ESS), the RES can provide the required power for the consumer stably, but the RES is usually connected to the dc bus through dc–dc converter system without PPP characteristic. Therefore, in this article, a novel PPP structure, which can embed the RES and the ESS, is proposed for the islanded dc microgrid with robust dc-link voltage. Notably, this structure can deal with the small difference among different RES units as well as the difference between the total output power of RESs and the required power of consumer. Besides, in the proposed PPP structure, the RES should feature the limited range of voltage regulation such as photovoltaic (PV) and fuel cell. Then, the control requirement of the RES and the robust dc-link voltage can both be achieved. In addition, based on the dual-active-bridge (DAB) dc–dc converter, a DAB-based PPP converter system is proposed for verifying the effectiveness of the proposed PPP structure. Then, a high-robustness control scheme is proposed for maintaining the total dc-link voltage when the working condition of the RES, the output voltage of the ESS, and the power requirement of the consumer are changed. Furthermore, when output power of one RES unit is limited, the corresponding operation is also proposed. Finally, by using PV panel as an example, simulation results and experiment results are provided to verify the effectiveness of the proposed PPP structure and the proposed methods.**

***Index Terms*—Islanded dc microgrid, partial power processing converter system, robustness dc-link voltage.**

Manuscript received 28 April 2022; revised 14 September 2022; accepted 28 October 2022. Date of publication 11 November 2022; date of current version 26 December 2022. This work was supported in part by the Future Energy Systems Initiative Funding from the Canada First Research Excellence Fund and in part by the Alberta Innovates Graduate Student Scholarship from the Alberta Innovates. Recommended for publication by Associate Editor K. A. Kim. *(Corresponding author: Yue Zhang.)*

Nie Hou, Li Ding, Pasan Gunawardena, Yue Zhang, and Yun Wei Li are with the Department of Electrical and Computer Engineering, University of Alberta, Edmonton, AB T6G 2V4, Canada (e-mail: nhou@ualberta.ca; lding@ualberta.ca; pasan@ualberta.ca; yue30@ualberta.ca; yunwei.li@ualberta.ca).

TianHong Wang is with the Department of Electrical Engineering, Southwest Jiaotong University, Chengdu 610031, China, also with the FEMTO-ST Institute UTBM, CNRS, Université Bourgogne Franche-Comté, F-90010 Belfort, France, and also with the Fédération de recherche Fuel Cell Lab UTBM, CNRS, Université Bourgogne Franche-Comté, F-90010 Belfort, France (e-mail: tianhong.wang@utbm.fr).

Color versions of one or more figures in this article are available at https://doi.org/10.1109/TPEL.2022.3221349.

Digital Object Identifier 10.1109/TPEL.2022.3221349

I. Introduction

With the appeal of carbon neutrality, the development of the renewable energy source (RES) has steadily increased over recent years [1]. Among the renewable energy sources such as photovoltaics (PV) and fuel cell (FC), PV energy has become one of the most important energy sources, especially for the residential PV grid-tied system [2], [3], the railway electrification system [4], and the electric vehicles charger system [5]. In most applications, PV panels are connected in series for achieving higher voltages as shown in Fig. 1(a) [6], [7]. However, because of some undesired factors such as manufacturing tolerances, partial shading, and nonuniform aging, the caused mismatch in the PV cells will restrict the total output power of these current-sharing panels.

Although the bypass diodes as shown in Fig. 1(a) can reduce the loss of the output power, the power losses are still high without a positive control, especially for the series-connected PV panels since the total available power of one cell-string may be bypassed for a small difference [8]. Moreover, with bypass diodes, the power-voltage curve will become complicated with several peak points, so it will be more difficult to realize the global maximum power transmission for the PV system [9]. To deal with this issue, the differential power processing (DPP) technique is a promising technique for realizing the individual maximum power point tracking (MPPT) control [10], [11], [12], where the DPP modules are isolated dc–dc converters. These isolated converters are employed to process only the mismatching power among PV panels under the MPPT controls, which can reduce the power rating of these converters and improve the efficiency of the PV-based system [13]. The typical DPP architectures can be shown in Fig. 1(b) as the PV-to-isolated port (PV-IP) structure and Fig. 1(c) as the PV-bus structure. In the PV-IP architecture, the string current is determined by the output power of the PV panels with MPPT, and the string current of the PV-bus structure can be adjusted flexibly. Thus, by optimizing the string current of PV-bus architecture, the efficiency of the PV-bus architecture can be higher than that of the PV-IP structure [14], [15]. For these distributed PV architectures as shown in Fig. 1, the total transferred current to the dc-link terminal is only from the PV modules, and under MPPT performance, this current is uncontrollable. Therefore, although there are lots of published articles focusing on the partial power processing

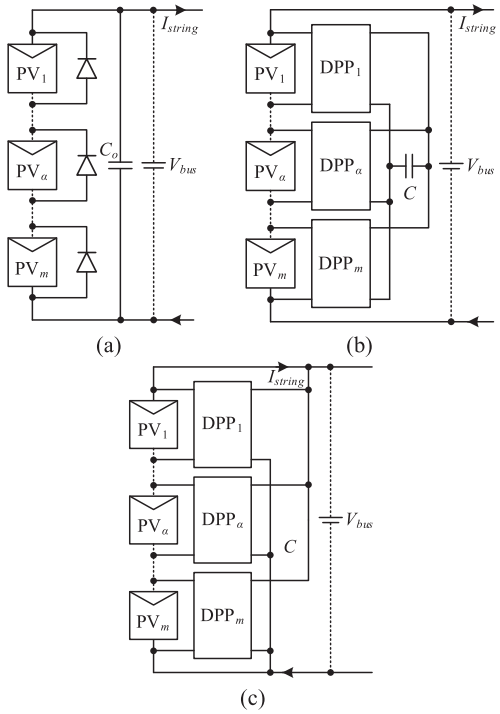

Fig. 1. Existing distributed PV architectures. (a) PV-D structure. (b) PV-IP structure. (c) PV-Bus structure.

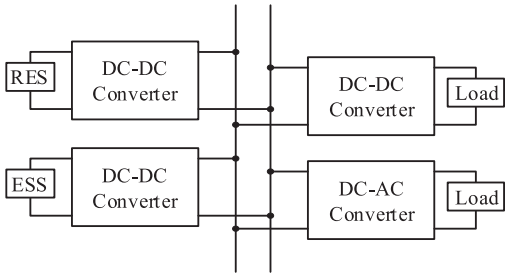

Fig. 2. Diagram of traditional RES-ESS based energy system for the islanded dc microgrid.

(PPP) structures for RES, there is not published article which can provide the constant dc-link voltage with the PPP technique.

Traditionally, combining the energy storage system (ESS) such as the battery, the RES such as PV and FC can provide the required power for the consumer stably, and the system configuration can be summarized in Fig. 2 [16], [18], [19]. A decentralized coordination power control scheme is proposed for islanding microgrids based on PV-battery configuration [16]. Similarly, a decentralized energy management scheme is proposed for the FC-battery based hybrid electric vehicle [19]. Compared with the centralized controller, the decentralized controller will usually limit the response capability of the converter system. Moreover, compared with the PPP structure for RES, the power loss will become bigger since there is always a dc–dc conversion stage between the RES and the dc terminal. Therefore, based on the compensated module (CM) for the total dc-link voltage, a novel PPP structure with adjustable dc-link voltage is proposed for islanded dc microgrid as shown in Fig. 3,

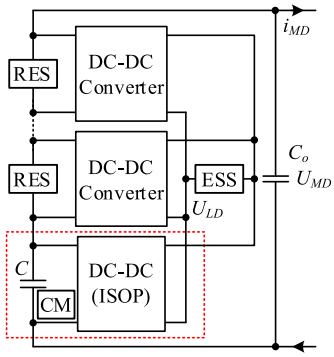

Fig. 3. Proposed PPP converter system with robust dc-link voltage for islanded dc microgrid.

which can deal with the small difference among different RESs as well as the difference between the total output power of the RES and the required power of consumer. Notably, if one CM cannot provide enough ability to maintain the total dc-link voltage, the input-series output-parallel (ISOP) CMs can be adopted.

Based on the dual-active-bridge (DAB) dc–dc converter, a DAB-based PPP converter system is proposed for verifying the effectiveness of the proposed PPP structure. Moreover, to boost the dynamic performance of this DAB-based converter system, a high robustness control scheme is proposed for maintaining the dc-link voltage under different conditions including changes of the RES working condition, the ESS output voltage, and the load consumer requirement. Furthermore, this proposed scheme can easily cooperate with the existing schemes for realizing the requirements of the RES, such as the maximum output power of PV panel and the desired output current of FC unit. In the following sections, the comparison between the traditional structure and the proposed structure is discussed in Section II. Then, the DAB-based PPP converter system is analyzed in Section III, and the adopted single-phase-shift (SPS) modulation method is also discussed. Then, the high-robustness control scheme is proposed in Section IV, and the operation, when the output power of one RES is limited, is also proposed. Finally, by using PV as an example, the simulation and experimental results are provided to validate the effectiveness of the proposed PPP converter system and the proposed high-robustness control scheme in Section V, followed by a conclusion in Section VI.

II. Comparison Between the Traditional Structure and the Proposed Structure

In this section, a comparison between the traditional RES-ESS based converter system and the proposed PPP converter system embedding the RES and the ESS is discussed, especially in terms of the effective energy and the cost.

A. Comparison of the Power Flow Condition

Moreover, the power flow conditions of the traditional RES-ESS system and the proposed RES-ESS system can be shown in Fig. 4. In the traditional system, a part of renewable energy can transfer to the load through one-stage dc–dc conversion

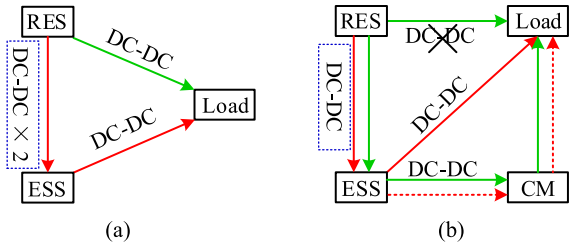

Fig. 4. Diagrams of the power flow condition. (a) The traditional system. (b) The proposed system.

as shown in Fig. 4(a). In the proposed system as shown in Fig. 4(b), this part of power is divided into two parts. A portion of power is directly transferred from the RES to load without dc–dc converter. Meanwhile, the other portion is transferred to the ESS and then to the load, which contains a two-stage dc–dc conversion. Therefore, when the voltage of CM is smaller than the half of the total dc-link voltage, the instantaneous power transmission between the RES and the load in the proposed PPP system will contain less dc–dc conversion than that in the traditional RES-ESS system. In addition, the other part of power in the RES is stored to the ESS and then transferred to the load. In the traditional system, this part of power will pass through a three-stage dc–dc conversion in the traditional system, while this part of power will only follow through a two-stage dc–dc conversion in the proposed system. Furthermore, the output voltages of the RES such as PV and FC are relatively smaller than the common dc-bus voltage [20], [21], so this proposed PPP structure is very suitable for the RES application in islanded dc microgrid with high-voltage terminal.

B. Comparison of Effective Energy

Since there are some powers charging in the ESS and then providing powers to the load consumer, instantaneous efficiency is meaningless. So, effective energy is adopted to compare the traditional structure and the proposed structure, and the effective energy is the energy which can be finally transferred to the load side from the original RES. Then, when μ of the total energy is transferred to the load from the RES, the energy flowing condition of the traditional RES-ESS based structure can be shown in Fig. 5(a). Furthermore, when λ of the energy, which is transferred to the load from the RES, is transferred to load consumer directly in the proposed structure, the energy flowing condition of the proposed PPP structure embedding the RES and ESS can be shown in Fig. 5(b).

Assuming the efficiency of each dc–dc conversion is the same as η, the unified effective energy of the traditional structure e_{tra} can be calculated as follows:

$$e_{\mathrm{tra}} = (1-\mu)\eta^3 + \mu\eta \qquad (0<\mu<1, 0<\eta<1). \tag{1}$$

Similarly, the unified effective energy of the proposed structure e_{pro} can be calculated as follows:

$$e_{\mathrm{pro}} = (1-\mu)\eta^2 + \mu(1-\lambda)\eta^2 + \mu\lambda \qquad (0<\lambda\leq 1) \tag{2}$$

where λ is the proportion of energy which directly transferred to load consumer in the load required power. Assuming e_{pro} is

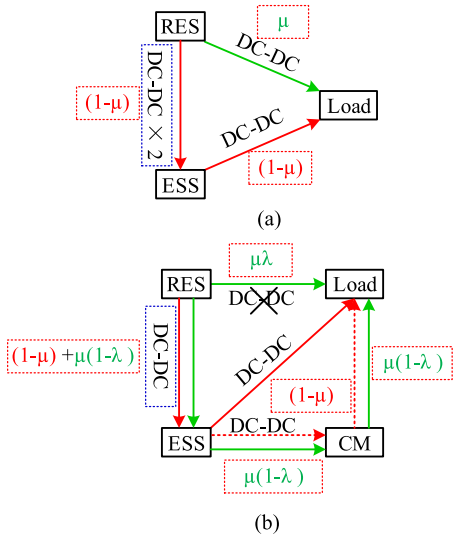

Fig. 5. Power flowing conditions under different structures. (a) The traditional structure. (b) The proposed structure.

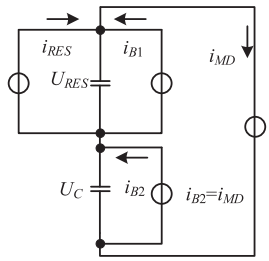

Fig. 6. Current flowing condition of the proposed PPP structure.

larger than e_{tra}, λ can be calculated as follows:

$$\lambda > \frac{(1-\mu)\eta^3 + \mu\eta - (1-\mu)\eta^2 - \mu\eta^2}{\mu - \mu\eta^2}. \tag{3}$$

Assuming the efficiency η of one dc–dc conversion is 95% and 50% of power from RES is only transferred to load ($\eta = 95\%$, $\mu = 50\%$), λ can be further calculated as follows:

$$\lambda > 0.0244. \tag{4}$$

When the output current of RES i_{RES} is bigger than the load current i_{MD}, λ can be regarded as the proportion of the total RES's voltage U_{RES} in the total dc-link voltage U_{MD} as shown in Fig. 6. When the output current of RES i_{RES} is lower than the load current i_{MD}, the proportion of the total RES's voltage U_{RES} in total dc-link voltage U_{MD} should be higher than λ. In this condition, assuming the average output current of RES i_{RES} is $1/2 i_{MD}$, the total RES's voltage U_{RES} should be 2λ of the total dc-link voltage U_{MD}. Furthermore, assuming the time when $i_{\mathrm{RES}} > i_{MD}$ is half of the day, the average voltage of the RES U_{RES} should be calculated as follows:

$$U_{\mathrm{RES}} = \frac{2\lambda U_{MD}}{2} + \frac{\lambda U_{MD}}{2} = \frac{3\lambda U_{MD}}{2} = 3.6\% U_{MD}. \tag{5}$$

According to (5), when the total RES's voltage URES is more than 3.6% of the total dc-link voltage UMD, the effective energy of the proposed structure will be bigger than that of

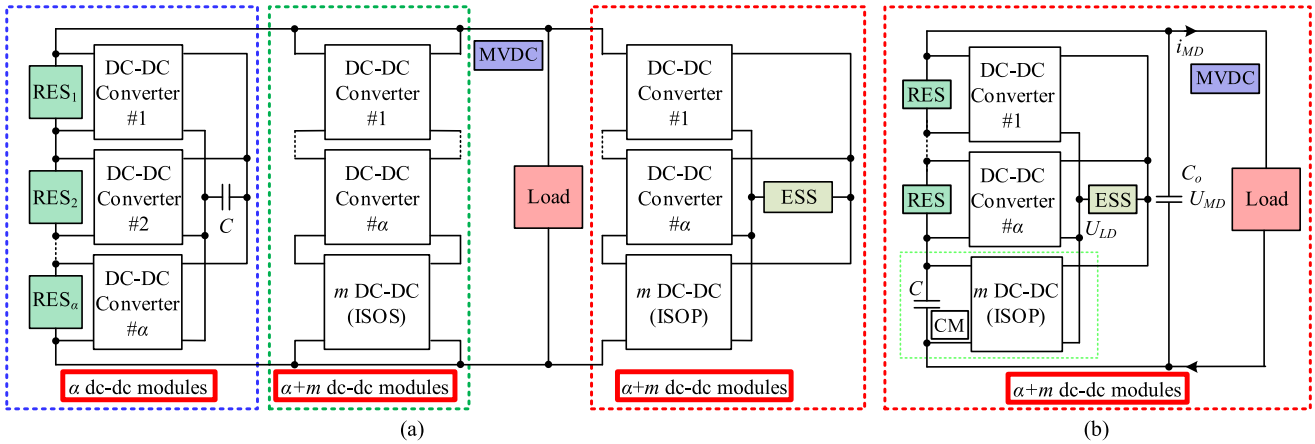

Fig. 7. Islanded dc microgrids with different structures. (a) The traditional RES-ESS based dc microgrid. (b) The proposed PPP converter system.

the traditional structure. Although this calculation is a little rough, this result also indicates that the proposed PPP structure embedding the RES and ESS has obviously advantage in the efficient use of renewable energy.

C. Comparison of the Cost

Assuming the voltage levels of RES and ESS are similar and the switches with the same rated voltage are used, the converter system for the traditional RES-ESS based structure and the proposed PPP structure embedding RES and ESS can be shown in Fig. 7 with α RES and one ESS, where α RESs and one ESS are adopted for meeting the requirement of the load consumer.

As shown in Fig. 7(a), by using switches with same rated voltage, $3\alpha+2m$ dc–dc modules are required in the traditional RES-ESS structure, while only $\alpha+m$ dc–dc modules are required in the proposed PPP structure as shown in Fig. 7(b). The current stress and voltage stress of the dc–dc converters between the RES and the dc-link terminal, and between the dc-link terminal and the ESS are similar as the current stress of the dc–dc converters in the proposed PPP structure, so the cost of the proposed PPP structure is far cheaper than that of the traditional structure. Moreover, there are three different dc–dc modules in the traditional structure, and the proposed structure only needs the same dc–dc module. So, the design cost of the proposed one is also cheaper than that of the traditional one.

In addition, these three different dc–dc stages in the traditional structure needs different control operations, while there is only one dc–dc stages with similar control requirement in the proposed PPP converter system. Therefore, the design of the control system of the traditional structure is more complicated than the proposed PPP structure. Then, the comparison between the traditional structure and the proposed structure can be summarized in Table I. With low cost, high effective energy, and simple control requirement, the advantages of the proposed PPP structure embedding the RES and ESS are obvious.

TABLE I
COMPARISON BETWEEN THE TRADITIONAL STRUCTURE AND PROPOSED STRUCTURE

Solution	Cost	Effective Energy	Electrical Stresses	Control System
Proposed Structure	**Low**	**High**	Similar	**Simple**
Traditional Structure	High	Low	Similar	Complicated

III. ANALYSIS OF THE DAB-BASED PPP CONVERTER SYSTEM

In this section, based on the proposed PPP structure, the DAB-based PPP structure is obtained and analyzed, and the average model of this converter system will be discussed. Then the SPS modulation is adopted for realizing the bidirectional power transmission of each DAB module.

A. DAB-Based PPP Converter System

Currently, the DAB dc–dc converter with the symmetric, isolated, and bidirectional characteristics becomes a promising candidate for the dc power system [22], which can form cascading or paralleling configurations for different voltage-level requirements. Moreover, since the soft switching performance can also be easily implemented, the high efficiency and high-power density are the advantages of this converter. In addition, the ultrafast dynamic performance under input-voltage or load disturbances of the DAB dc–dc converter can be easily achieved, which can boost the robustness of the dc microgrid [23], [24], [25]. Then, based on the proposed PPP structure, the DAB-based PPP converter system can be shown in Fig. 8 with the consideration of one CM. As shown in Fig. 8, the mth DAB module is adopted to adjust the total dc-link voltage, and other DAB modules are employed to meet the requirement of the RES such as maximum output power of PV and the desired output current of fuel cell. Besides, if one compensated DAB module cannot provide the enough ability to maintain the total dc-link voltage, the input-series output-parallel (ISOP) DAB modules can be adopted.

B. Average Model of DAB-Based PPP Converter System

Traditionally, the inductance of the dc–dc converter such as buck and boost plays an important role in the modeling analysis. Nevertheless, since the transferred current of the DAB dc–dc

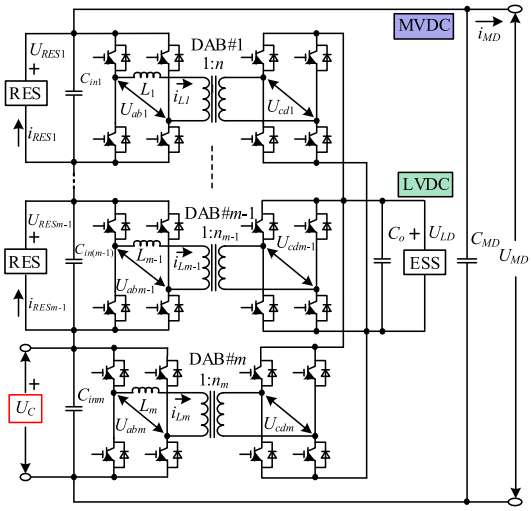

Fig. 8. Topology of the proposed DAB-based PPP converter system with adjustable dc-link voltage.

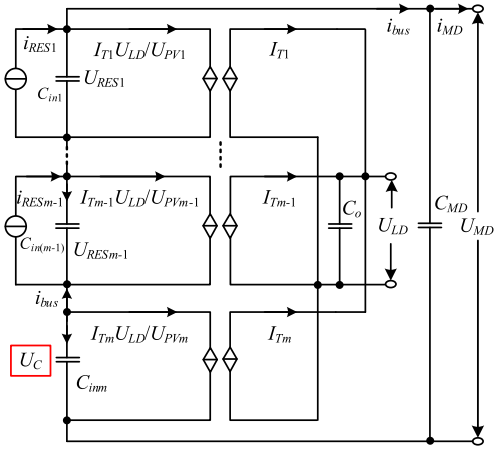

Fig. 9. Simplified circuit of the DAB-based PPP converter system with battery integration.

converter can be determined by the circuit parameter and the phase-shift ratio, the middle ac inductance can be neglectful [24], [26]. So, the DAB converter can be treated as a controllable current source by using different control values. Moreover, the RES such as PV and FC can usually be modeled as a current source [27], [28], [29], and the ESS such as a battery is a voltage source. Then, the simplified circuit of the DAB-based PPP converter system can be shown in Fig. 9. According to Fig. 9, the average model of the DAB-based PPP converter system can be expressed as follows:

$$\begin{cases} C_{\text{in}\alpha}\frac{dU_{\text{RES}\alpha}}{dt} = i_{\text{RES}\alpha} - i_{\text{bus}} - \frac{I_{T\alpha}U_{LD}}{U_{\text{RES}\alpha}} \\ C_{\text{in}m}\frac{dU_C}{dt} = -\frac{I_{Tm}U_{LD}}{U_C} - i_{\text{bus}} \\ C_{MD}\frac{dU_{MD}}{dt} = i_{\text{bus}} - i_{MD} \\ U_{MD} = U_C + \sum_{\alpha=1}^{m-1} U_{\text{RES}\alpha} \end{cases} \quad (\alpha \in [1, m-1]) \quad (6)$$

where $C_{\text{in}\alpha}$ and $C_{\text{in}m}$ are the input capacitors of DAB modules, $U_{\text{RES}\alpha}$ is the voltage of the RES, i_{bus} is the current between the DAB module and the total dc link, $I_{T\alpha}$ and I_{Tm} are the

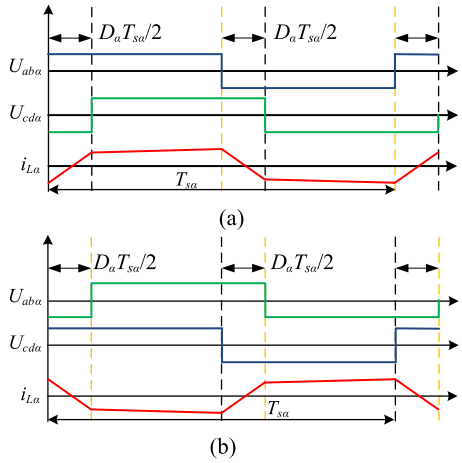

Fig. 10. SPS modulation method of the DAB converter for bidirectional power flowing conditions. (a) DABs transfer power to the battery. (b) DABs absorb power from the battery.

transferred current of the DAB modules, C_{MD} is the capacitor of the total dc link, U_{MD} is the total dc-link voltage, i_{MD} is the load current and U_{LD} is the output voltage of the ESS. Based on (6), the transferred current of the first (m–1)th DAB modules can be employed to adjust the output voltage $U_{\text{RES}\alpha}$ for meeting the requirement of the RES such as the maximum output power of PV and the desired output current of FC. Besides, to maintain the dc-link voltage U_{MD}, the input voltage U_C of the compensated DAB module should be controlled, which can be realized by adjusting the transferred current I_{TM} of this DAB module.

C. Single-Phase-Shift Modulation Method

For the DAB dc–dc converter, the SPS modulation method is the most popular modulation method for realizing the flexible power transmission. Thus, in this article, the SPS modulation method is adopted, which can be illustrated in Fig. 10 for bidirectional power transmission, where $U_{ab\alpha}$ is the output voltage of the primary-side H Bridge, $U_{cd\alpha}$ is the output voltage of the secondary-side H Bridge, $i_{L\alpha}$ is the inductance current, D_α is the phase-shift ratio, and $T_{s\alpha}$ is the switching period of the corresponding DAB modules.

According to Fig. 10, the transferred power P_α of DAB module connected to the RES under SPS modulation method can be expressed as follows:

$$P_\alpha = \begin{cases} \frac{U_{\text{RES}\alpha}U_{LD}D_\alpha(1-D_\alpha)T_{s\alpha}}{2n_\alpha L_\alpha} & (P_\alpha \geq 0) \\ -\frac{U_{\text{RES}\alpha}U_{LD}D_\alpha(1-D_\alpha)T_{s\alpha}}{2n_\alpha L_\alpha} & (P_\alpha < 0). \end{cases} \quad (7)$$

Then, the transferred current $I_{T\alpha}$ of the DAB module can be expressed as follows:

$$I_{T\alpha} = \frac{P_\alpha}{U_{LD}} = \begin{cases} \frac{U_{\text{RES}\alpha}D_\alpha(1-D_\alpha)T_{s\alpha}}{2n_\alpha L_\alpha} & (I_{T\alpha} \geq 0) \\ -\frac{U_{\text{RES}\alpha}D_\alpha(1-D_\alpha)T_{s\alpha}}{2n_\alpha L_\alpha} & (I_{T\alpha} < 0). \end{cases} \quad (8)$$

As shown in (8), the transferred current of the DAB module connected to the RES can be directly calculated by the phase-shift ratio, which is also suitable for the DAB module for

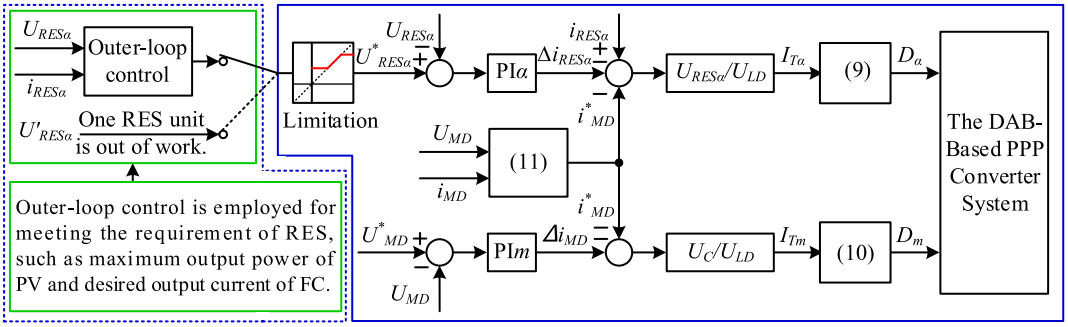

Fig. 11. Control diagram of the proposed high-robustness control scheme for the DAB-based PPP converter system.

compensating the total dc-link voltage. Therefore, if the desired transferred current for each DAB module can be obtained, the required phase-shift ratio can be directly obtained for realizing this transferred current. Furthermore, when the desired current can balance the relationship between the output current of the RES and the load requirement of current, the fast-dynamic performance can be easily obtained, and the robustness of the total dc-link voltage can be ensured.

IV. Proposed High-Robustness Control Strategy

In this section, a high-robustness control scheme is proposed to boost the dynamic response of the DAB-based PPP converter system. When the working condition of the RES, the output voltage of the ESS, the required power of the load consumer are changed, this proposed scheme is employed to maintain the total dc-link voltage. Moreover, the operation, when one RES unit is out of work, is also discussed for ensuring the reliability of the proposed DAB-based PPP converter system.

A. Proposed High-Robustness Control Scheme

As analysis in the last section, the DAB module can be treated as a controllable current source, so the direct current control scheme is very suitable for the DAB-based converter system [30]. Then, based on the desired transferred current, the phase-shift ratio D_α in (8) can be calculated by the required transferred current as follows:

$$D_\alpha = \begin{cases} \frac{1}{2} - \sqrt{1 - \frac{8L_\alpha I_{T\alpha}}{n_\alpha U_{\mathrm{RES}\alpha} T_{s\alpha}}} & (I_{T\alpha} \geq 0) \\ \frac{1}{2} - \sqrt{1 + \frac{8n_\alpha L_\alpha I_{T\alpha}}{U_{\mathrm{RES}} T_{s\alpha}}} & (I_{T\alpha} < 0). \end{cases} \tag{9}$$

Similarly, the phase-shift ratio D_m of the mth DAB module can be expressed by its transferred current I_{Tm} as follows:

$$D_m = \begin{cases} \frac{1}{2} - \sqrt{1 - \frac{8L_m I_{Tm}}{n_m U_C T_{sm}}} & (I_{Tm} \geq 0) \\ \frac{1}{2} - \sqrt{1 + \frac{8n_m L_m I_{Tm}}{U_C T_{sm}}} & (I_{Tm} < 0). \end{cases} \tag{10}$$

Moreover, according to Fig. 9, to meet the requirement of the load side, the bus current i_{bus} should be equivalent to the load current i_{MD}. To immediately track the change of load, the required current i^*_{MD} of each DAB module for supporting the electricity consumption can be expressed as follows:

$$i^*_{MD} = \frac{U^*_{MD} i_{MD}}{U_{MD}}. \tag{11}$$

Then, combining (6), (9)–(11), the high-robustness control scheme for the DAB-based PPP converter system can be illustrated as Fig. 11. For the DAB module connected with the RES, the desired terminal voltage can be obtained from outer loop control for the RES, such as the maximum output power of the PV [28] and the desired output current of the FC [29]. Moreover, the CM is employed to regulate the total dc-link voltage directly. Since the CM needs to compensate the total dc-link voltage for several RES units, the overvoltage of the CM may be emerged. Therefore, to avoid the potential overvoltage, the desired terminal voltage of the RES should be limited. Meanwhile, under normal condition, the requirement of the voltage regulating range for the RES should also be limited.

At the beginning of each switching period, the output current of each RES unit, the terminal voltage of each RES unit, the input voltage of the CM, the load current, the output voltage of the ESS, and the total dc-link voltage are measured. Then based on the output current and the terminal voltage of each RES unit, the desired terminal voltage can be obtained for meeting the requirement of the RES, such as the maximum output power of the PV and the desired output current of the FC. In addition, based on the load current and the total dc-link voltage, the desired output current for supporting the load consumer can be obtained as (11). For the DAB module connected with the RES, the total transferred current can be obtained by combining the current which is employed to adjust the RES's voltage by (6). This current can be obtained through the corresponding PI controller with the terminal voltage and the desired voltage of the RES. Similarly, by combining the current for maintaining the dc-link voltage from the mth PI controller, the transferred current for the additional DAB dc–dc converter can be obtained. Furthermore, based on (9) and (10), the required phase-shift ratio for each DAB module can be obtained, which can be used to realize the control of the DAB-based PPP converter system. Then, the proposed high robustness control scheme can be realized for controlling this DAB-based PPP converter system when the working condition of the RES, the output voltage of the ESS, and the power requirement of the consumer are changed.

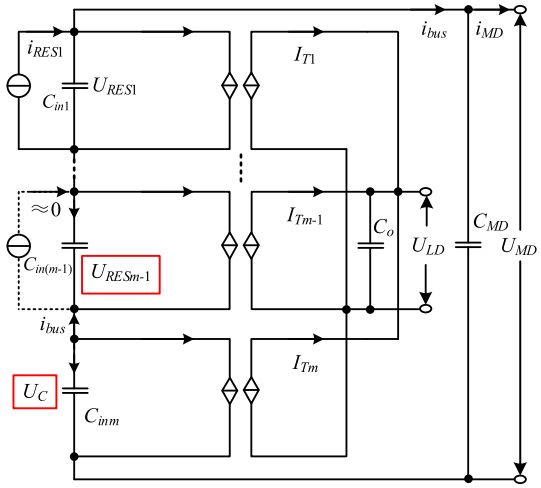

Fig. 12. Simplified circuit of the DAB-based PPP converter system when one RES unit is out of work.

For the single-phase-shift modulation method, the PI parameters k_p and k_i can be calculated as follows [30]:

$$\begin{cases} k_p \le \left| \frac{\Delta D_{\min} U_{\text{in}} T_s}{nLU_{omn}} \sqrt{\frac{1}{4} - \frac{2nLI_T}{U_{\text{in}} T_s}} \right| \\ k_i \le \left| \frac{\Delta D_{\min} U_{\text{in}} T_s}{10nLU_{omn}} \sqrt{\frac{1}{4} - \frac{2nLI_T}{U_{\text{in}} T_s}} \right| \end{cases} \tag{12}$$

where $\Delta D_{\min}$ is the limitation of phase-shift disturbance, U_{in} is the input voltage, I_T is the corresponding transferred current, U_{omn} is the measurement noise, n is the transformer turn ratio, L is the inductance, and T_s is the switching period.

B. Operation When One RES Unit is Out of Work

Sometimes, when one RES unit is out of work such as the PV panel at night and the FC without burning material, the output current of this RES unit will become very small. If the desired terminal voltage of the RES-connected DAB module is still dependent on the requirement of the RES, the converter system will become unstable since the control purpose of the RES becomes meaningless. Therefore, to deal with this issue, this DAB module should be turned into constant voltage control, and the desired voltage will be constant when the RES unit is out of work. Then, the simplified circuit of the DAB-based PPP converter system can be shown in Fig. 12. As shown in Fig. 12, when one RES unit is out of work, the ESS will provide the total power to support the terminal voltage. Similarly, when all the RES units are out of work such as the PV panels at night, only the ESS will provide the power to the load consumer.

C. Required Characteristics of the RES for the Proposed High-Robustness Control Scheme

The RES should feature current output, and if the RES features voltage output, there will be no control goal for the DAB module which is connected to the RES. Moreover, under normal working condition, the regulating range of the desired terminal voltage is limited, which ensures that the overvoltage of the CM can be avoidable. Furthermore, with this characteristic, one CM can compensate the voltage change of more RES units, and less power between the RES and the load will follow through the dc–dc converter. In addition, the relationship among the output current, the terminal voltage, and the output power of the RES should be regular, and then, the control of the RES can be equivalent to the control the terminal voltage.

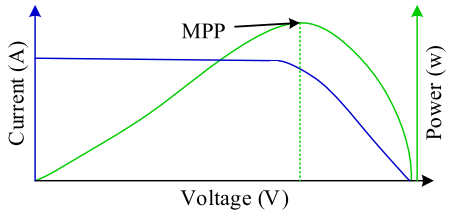

Fig. 13. Typical output characteristic of PV panel.

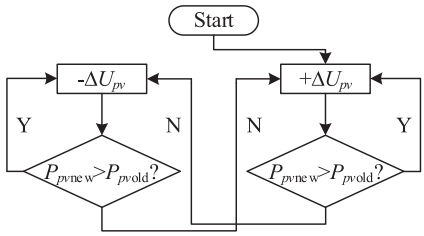

Fig. 14. Basic block diagram of P&O MPPT.

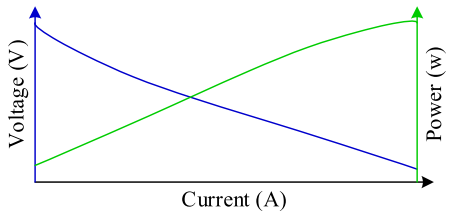

Fig. 15. Typical output characteristic of the FC stack.

For example, the typical output characteristic of PV panel can be shown in Fig. 13, where the relationship among the output current, the terminal voltage, and the output power can be obtained. When the terminal voltage is increased from zero, the output power is increased at first, and then, the maximum power point (MPP) can be obtained. Furthermore, the output power of the PV will be decreased along with the increasing of the terminal voltage. Therefore, by adjusting the terminal voltage, there are lots of existing schemes for studying the MPPT performance of PV panel. Generally, when the temperature (–25°C 75°C) and the irradiance (200–1000 W/m^2) of PV panel is changed from, the change of the output voltage is about 30% for maximum output power [31], [32]. Therefore, the PV panel meets the required characteristics of the proposed high-robustness control scheme. Moreover, perturb and observe method or the hill climbing method is the widely used technique to track the maximum output power of PV panels as shown in Fig. 14 [33], [34], which can act as the outer loop control for the PV-based PPP converter system.

In addition, the typical output characteristic of proton exchange membrane FC stack can be shown in Fig. 15 [35], [36],

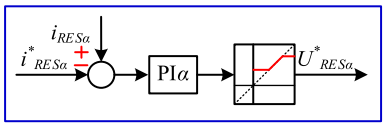

Fig. 16. Outer current-loop control for the FC stack.

where the relationship among the output current, the terminal voltage, and the output power can be obtained. When the output current is increased from zero, the terminal output voltage is reduced, and the output power of the FC stack is increased. Notably, to avoid overcurrent of FC stack, the output current becomes the prior control purpose, which is usually realized by adjusting the terminal voltage. Therefore, by adjusting the terminal voltage, the desired output current of the FC can be implemented. Generally, when the output current of the FC is changed in a large range, the change rate of the terminal voltage is smaller than 30%. Therefore, the FC stack meets the required characteristics of the proposed high-robustness control scheme. Moreover, to realize the regulation of the FC, the current control can act as the outer-loop control for FC-based PPP converter system, which can be simplified as shown in Fig. 16. Since the output current and the terminal voltage of the FC stack is inversely proportional, the output current should be the positive feedback for cooperating with the proposed high-robustness control scheme.

V. Verification

In this section, by using PV panel as an example, a simulation model with three DAB modules and a small-scale experiment platform with two DAB modules is built to verify the effectiveness of the proposed PPP structure, the high-robustness control strategy, and the proposed operation when one RES unit is out of work.

A. Simulation Results With Two PV Panels and One Compensating Module

In this part, a simulation model with three DAB modules is built. Since the ESS such as battery can be also switched into a low-voltage dc bus, a dc voltage source is employed to replace the ESS for testing the function of this proposed converter and the corresponding control method. The circuit parameters of the converter system with two modules are shown in Table II.

When the battery voltage U_{LD} is 90 V and the load resistor R is 150 Ω, Fig. 17 shows the simulation result with changed irradiances of PV panels. As shown in Fig. 17(a), the irradiance of the first PV panel is changed from 600 to 560 W/m^2 then to 600 W/m^2, and the irradiance of the second PV panel is increased from 520 to 560 W/m^2 then to 600 W/m^2. Then, the desired output voltages of PV panels can be shown in Fig. 17(b), and the corresponding output current of PV panels can be shown in Fig. 17(c). Based on the proposed high robustness control scheme, the output voltages of PV panels and the compensated voltage can be shown in Fig. 17(d), and the total dc-link voltage U_{MD} can be obtained as shown in Fig. 17(e). Thus, based on

TABLE II
Circuit Parameters of Simulation Model

L_1, L_2, L_3	4mH
n_1, n_2, n_3	1/5
f_s	1 kHz
R	150–300Ω
U_{LD}	80–90V
U^*_{MD}	1000 V
Modules of PV1 in series	14
Modules of PV2 in series	13
PV1, PV2	Trina Solar TSM-250PA05.08

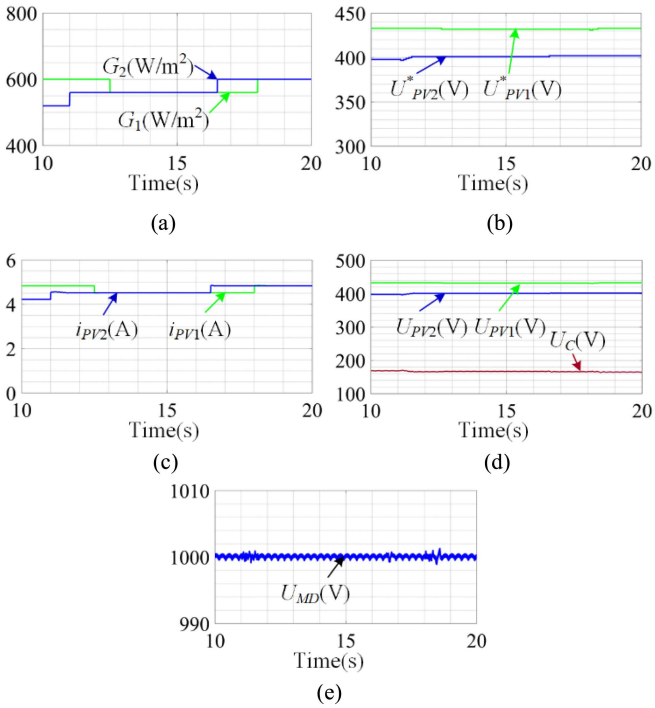

Fig. 17. Simulation results when the irradiances are changed. (a) Irradiance. (b) Desired PV voltage. (c) Output current of PV. (d) Voltages for each DAB. (e) The total dc-link voltage.

the proposed control method, the robustness of the total dc-link voltage can be ensured when the irradiances of PV panels are changed.

Moreover, when the irradiance of the first PV panel is 600 W/m^2 and the irradiance of the second PV panel is 520 W/m^2, Fig. 18 shows the simulation result with a changed load resistor. As shown in Fig. 18(a), the load resistor is changed between 150 and 300 Ω. Based on the proposed high robustness control scheme, the output voltages of PV panels and the compensated voltage can be shown in Fig. 18(b), and the total dc-link voltage U_{MD} can be obtained as shown in Fig. 18(c), where the total dc-link voltage is maintained at its desired value. Therefore, based on the proposed control method, excellent dynamic performance can be provided for the presented DAB-based PPP converter system when the load resistor is changed.

In addition, when the irradiance of the first PV panel is 600 W/m^2 and the irradiance of the second PV panel is

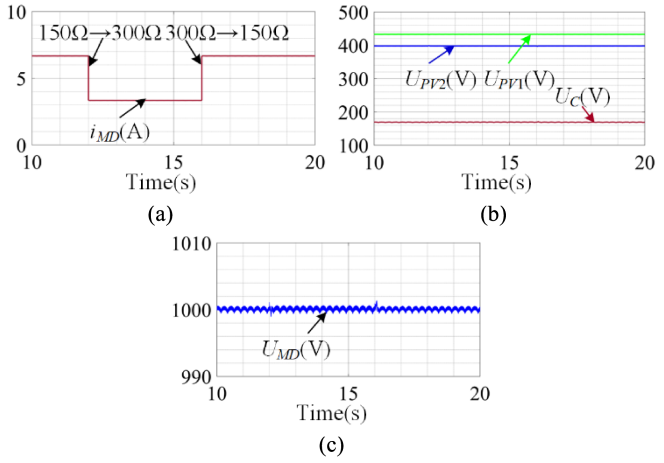

Fig. 18. Simulation results when load resistor is changed. (a) Output current of dc bus. (b) Voltages for each DAB. (c) The total dc-link voltage.

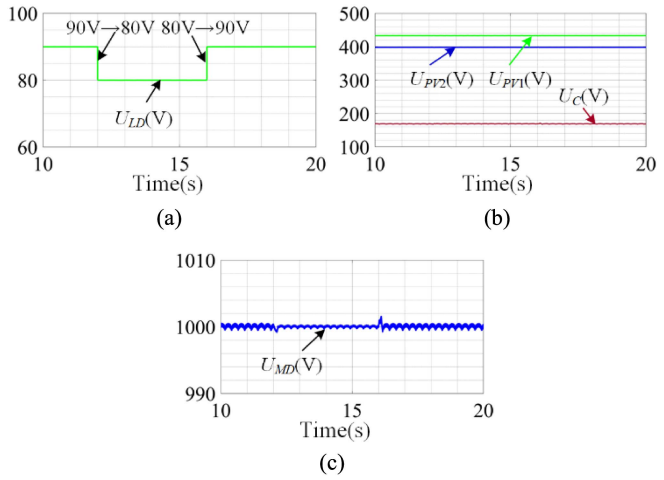

Fig. 19. Simulation results when voltage of the ESS is changed. (a) Voltage of the ESS. (b) Voltages for each DAB. (c) The total dc-link voltage.

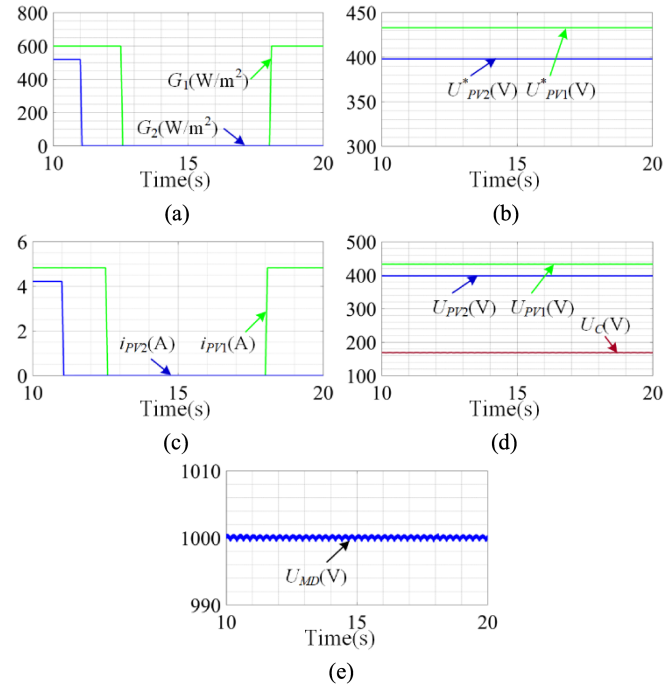

Fig. 20. Simulation results when the PV panel is covered. (a) Irradiance. (b) Desired PV voltage. (c) Output current of PV. (d) Voltages for each DAB. (e) The total dc-link voltage.

TABLE III
CIRCUIT PARAMETERS OF THE ADOPTED SMALL-SCALE EXPERIMENT PLATFORM

L_1, L_2	40 μH
n_1, n_2	1
f_s	40 kHz
R	40–90Ω
U_{LD}	50–60 V
U^*_{MD}	100 V
P_{MD}	111–250 W

520 W/m^2, Fig. 19 shows the simulation result with a changed voltage of the low-voltage bus. As shown in Fig. 19(a), the voltage of the low-voltage bus is changed between 80 and 90 V. Based on the proposed high robustness control scheme, the output voltages of PV panels and the compensated voltage can be shown in Fig. 19(b). Then, as shown in Fig. 19(c), the total dc-link voltage can be kept at its desired value by using the proposed high robustness control scheme. Therefore, based on the proposed control method, excellent dynamic performance can be provided for the presented DAB-based PPP converter system when the voltage of the low voltage terminal is changed.

Furthermore, when the battery voltage U_{LD} is 90 V and the load resistor R is 150 Ω, Fig. 20 shows the simulation result when the PV panels are heavily covered sometimes. As shown in Fig. 20(a), the irradiance of the first PV panel become as zero at first and then return to 600 W/m^2 then to 600 W/m^2, and the irradiance of the second PV panel is reduced to zero without recovery. Then, combining the operation for the idle PV panel, the desired output voltages of PV panels can be shown in Fig. 20(b), and the corresponding output current of PV panels can be shown in Fig. 20(c). Based on the proposed high robustness control scheme, the output voltages of PV panels and the compensated voltage can be shown in Fig. 20(d), and the total dc-link voltage U_{MD} can be obtained as shown in Fig. 20(e). Thus, based on the proposed control method, the robustness of the total dc-link voltage can be ensured even when the PV panels are out of work.

B. Experiment Results With One PV Panel and One Compensating Module

In this part, a small-scale experiment platform with two DAB modules is built. The main circuit parameters of this experiment platform can be shown in Table III, where P_{MD} is the required power of load side. Moreover, the configuration of the small-scale experiment platform can be shown in Fig. 21, where the power supply Agilent E4360A is employed to simulate the PV panel and the power supply Sorensen SGX60X83C is used to

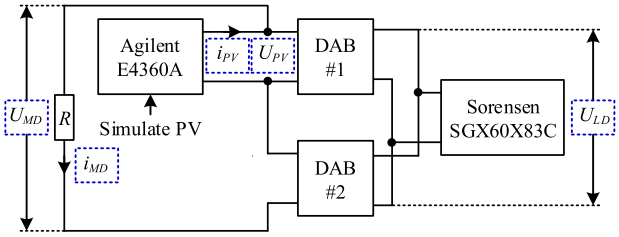

Fig. 21. Configuration of the small-scale experiment platform.

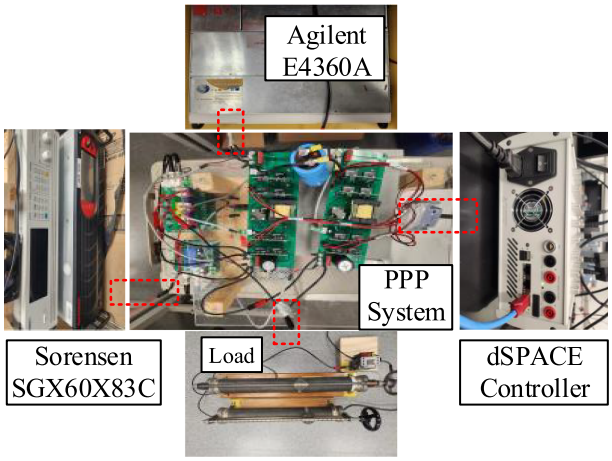

Fig. 22. Picture of the experiment platform.

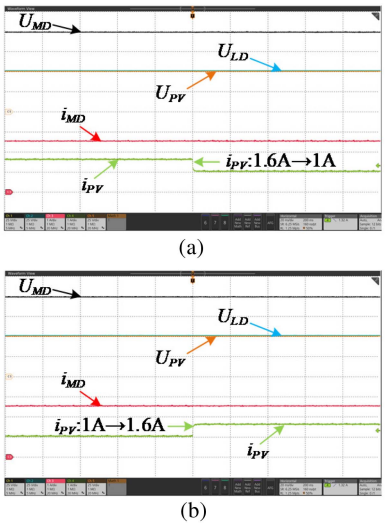

Fig. 23. Experiment results when the output current of the PV panel at MPP is changed (U_{MD}, $U_{\rm PV}$, and U_{LD}: 25 V/div; i_{MD} and $i_{\rm PV}$: 1 A/div; t: 20 ms/div). (a) i_{PV}: 1.6 A → 1 A. (b) i_{PV}: 1 A → 1.6 A.

replace the battery. As shown in Fig. 21, the total dc-link voltage U_{MD}, the load current i_{MD}, the output current $i_{\rm PV}$ of PV, the terminal voltage $U_{\rm PV}$ and the voltage U_{LD} are measured by an oscilloscope. The corresponding picture of the corresponding small-scale platform can be shown in Fig. 22.

When the load resistor is 40 Ω, the voltage of the ESS bus is 50 V and the PV voltage at MPP is 50 V, Fig. 23 shows the experiment results when the output current $i_{\rm PV}$ of PV panel is

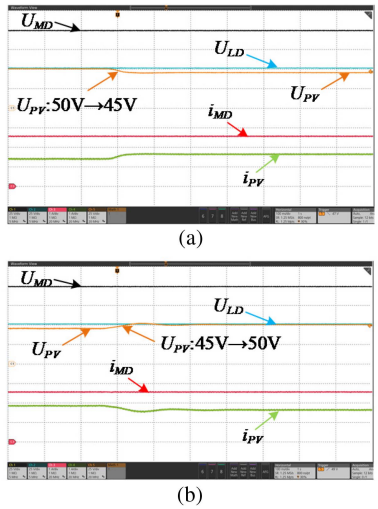

Fig. 24. Experiment results when the terminal voltage of PV panel at MPP is changed (U_{MD}, $U_{\rm PV}$, and U_{LD}: 25 V/div; i_{MD} and $i_{\rm PV}$: 1 A/div; t: 100 ms/div). (a) U_{PV}: 50 V → 45 A. (b) U_{PV}: 45 A → 50 A.

changed. As shown in Fig. 23, when the output current of the PV panel is changed between 1 and 1.6 A, the total dc-link voltage U_{MD} can be remained at its desired value by using the proposed high-robustness control scheme. Thus, when the output current of the PV panel is changed, excellent dynamic performance can be obtained by using the DAB-based PPP converter system with the proposed control scheme.

Moreover, when the load resistor is 40 Ω, the voltage of the ESS is 50 V and the PV current at MPP is 1.6 A, Fig. 24 shows the experiment result when the terminal voltage $U_{\rm PV}$ of the PV panel at MPP is changed. As shown in Fig. 24, when the output voltage of the PV panel is changed between 45 and 50 V, the total dc-link voltage U_{MD} can be remained at its desired value by using the proposed high-robustness control scheme. Thus, when the terminal voltage of the PV panel is changed, excellent dynamic performance can be obtained by the proposed control scheme.

In addition, when the voltage of the ESS is 50 V, the PV voltage is 50 V and the PV current at MPP is 1.6 A, Fig. 25 shows the experiment result when the load resistor R is changed. As shown in Fig. 25, when the load resistor is changed between 40 and 90 Ω, the total dc-link voltage U_{MD} can be remained at its desired value by using the proposed high-robustness control scheme. Then, when the load resistor is changed, excellent dynamic performance can be obtained by the proposed control scheme for the DAB-based PPP converter system.

Similarly, when the load resistor is 40 Ω, the PV voltage is 50 V and the PV current at MPP is 1.6 A, Fig. 26 shows the experiment result when the terminal voltage U_{LD} of the ESS bus is changed. As shown in Fig. 26, when this voltage is changed between 50 and 60 V, the total dc-link voltage U_{MD} can be remained at its desired value by using the proposed high-robustness control scheme. Then, when the terminal voltage of the ESS bus is changed, the excellent dynamic performance can be obtained by the proposed control scheme for the DAB-based PP P converter system.

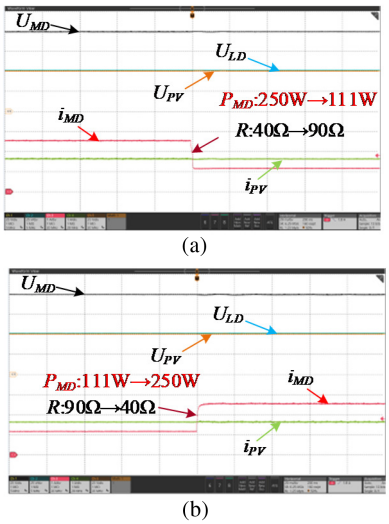

Fig. 25. Experiment results when the load resistor is changed (U_{MD}, $U_{\rm PV}$, and U_{LD}: 25 V/div; i_{MD} and $i_{\rm PV}$: 1 A/div; t: 20 ms/div). (a) R: 40 Ω → 90 Ω. (b) R: 90 Ω → 40 Ω.

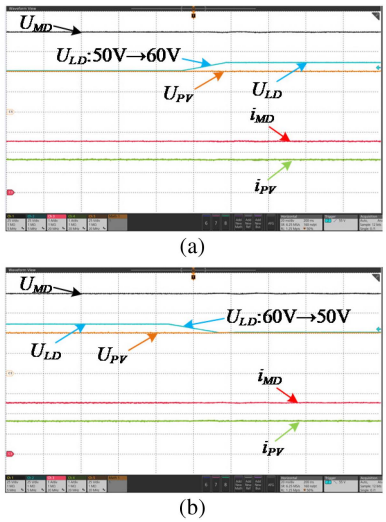

Fig. 26. Experiment results when the voltage of the ESS bus is changed (U_{MD}, $U_{\rm PV}$, and U_{LD}: 25 V/div; i_{MD} and $i_{\rm PV}$: 1 A/div; t: 20 ms/div). (a) U_{LD}: 50 V → 60 V. (a) U_{LD}: 60 V → 50 V.

Furthermore, when the load resistor is 40 Ω, the voltage of the ESS is 50 V, the output current of PV is 1.6 A and the PV voltage at MPP is 50 V, Fig. 27 shows the experiment results to simulate the transient processes when the PV panels are out of work or activated again. As shown in Fig. 27(a), when the PV panel is out of work, the output current suddenly becomes zero, and based on the high-robustness control scheme, the total dc-link voltage U_{MD} can be kept at its desired value. Then, as shown in Fig. 27(b), when the PV panel is activated again, the total dc-link voltage U_{MD} is also constant. Therefore, based on the proposed high-robustness control scheme, when the PV panel is out of work or activated suddenly, the excellent dynamic performance can be provided for the presented DAB-based PPP converter system.

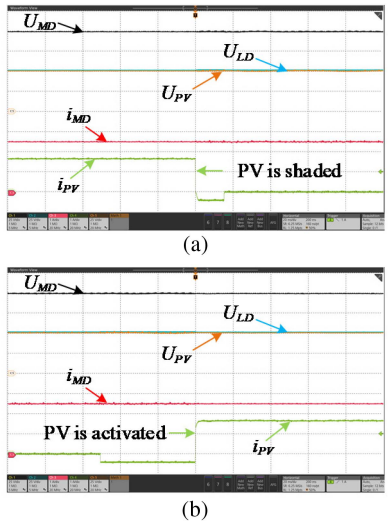

Fig. 27. Experiment results when the PV panel is out of work or activated again (U_{MD}, $U_{\rm PV}$, and U_{LD}: 25 V/div; i_{MD} and $i_{\rm PV}$: 1 A/div; t: 20 ms/div). (a) PV is out of work. (b) PV is activated.

VI. Conclusion

In this article, a partial power processing structure embedding the renewable energy source and the energy storage system is proposed for the islanded dc microgrid, which can also be an alternate scheme when the electricity consumer loses the support of the strong grid system. Then, based on the DAB modules, the DAB-based partial power processing converter system is proposed for verifying the effectiveness of the proposed partial power processing structure. Moreover, for this DAB-based converter system, a high-robustness control scheme proposed for maintaining the total dc-link voltage when the working condition of the renewable energy source, the output voltage of the energy storage system, and the load condition are changed. In addition, when one renewable energy source is out of work such as the PV panel at night and the FC without burning material, the corresponding operation is also proposed. Furthermore, the required characteristics of the RES for the proposed high-robustness control scheme are discussed. The conducted studies are summarized as follows.

1) By using the DAB-based partial power processing converter system as an example, the constant total dc-link voltage can be achieved, and the effectiveness of the proposed PPP structure is verified. Thus, by embedding the renewable energy source and the energy storage system, the proposed partial power processing converter system in this article can be employed to provide the constant dc-link voltage for the islanded dc microgrid.
2) Based on the proposed high-robustness control scheme, the excellent dynamic response can be provided for the DAB-based partial power processing converter system when the working condition of PV panel, the voltage of the battery and the condition are changed. Moreover, when one renewable energy source such as PV panel is out of work, the total dc-link voltage can still be stable by using the proposed operation.

3) In the proposed partial power processing structure, the renewable energy source should feature the current output and the limited requirement of the terminal voltage regulation. Moreover, to realize the regulation on converter side, the relationship among the output current, the terminal voltage, and the output power of the renewable energy source should be regular.
4) Since the output voltages of the PV panel and the FC stack are usually smaller than the common dc-bus voltage, the proposed PPP structure is very suitable for these renewable energy sources, and the higher total dc-link and the higher power capacity can be obtained.

REFERENCES

[1] B. Liu, F. Zhuo, Y. Zhu, and H. Yi, "System operation and energy management of a renewable energy-based DC micro-grid for high penetration depth application," *IEEE Trans. Smart Grid*, vol. 6, no. 3, pp. 1147–1155, May 2015.

[2] Y. Li, D. M. Vilathgamuwa, and P. C. Loh, "Design, analysis, and real-time testing of a controller for multibus microgrid system," *IEEE Trans. Power Electron.*, vol. 19, no. 5, pp. 1195–1204, Sep. 2004.

[3] X. Li, L. Guo, C. Hong, Y. Zhang, Y. W. Li, and C. Wang, "Hierarchical control of multiterminal DC grids for large-scale renewable energy integration," *IEEE Trans. Sustain. Energy*, vol. 9, no. 3, pp. 1448–1457, Jul. 2018.

[4] X. Zhu, H. Hu, H. Tao, and Z. He, "Stability analysis of PV plant-tied MVdc railway electrification system," *IEEE Trans. Transp. Electrific.*, vol. 5, no. 1, pp. 311–323, Mar. 2019.

[5] V. M. Iyer, S. Gulur, G. Gohil, and S. Bhattacharya, "An approach towards extreme fast charging station power delivery for electric vehicles with partial power processing," *IEEE Trans. Ind. Electron.*, vol. 67, no. 10, pp. 8076–8087, Oct. 2020.

[6] A. Mäki and S. Valkealahti, "Power losses in long string and parallel-connected short strings of series-connected silicon-based photovoltaic modules due to partial shading conditions," *IEEE Trans. Energy Convers.*, vol. 27, no. 1, pp. 173–183, Mar. 2012.

[7] P. Manganiello, M. Balato, and M. Vitelli, "A survey on mismatching and aging of PV modules: The closed loop," *IEEE Trans. Ind. Electron.*, vol. 62, no. 11, pp. 7276–7286, Nov. 2015.

[8] L. Gao, R. A. Dougal, S. Liu, and A. P. Iotova, "Parallel-connected solar PV system to address partial and rapidly fluctuating shadow conditions," *IEEE Trans. Ind. Electron.*, vol. 56, no. 5, pp. 1548–1556, May 2009.

[9] M. O. Badawy, S. M. Bose, and Y. Sozer, "A novel differential power processing architecture for a partially shaded PV string using distributed control," *IEEE Trans. Ind. Appl.*, vol. 57, no. 2, pp. 1725–1735, Mar./Apr. 2021.

[10] Y. T. Jeon and J. H. Park, "Unit-minimum least power point tracking for the optimization of photovoltaic differential power processsing systems," *IEEE Trans. Power Electron.*, vol. 34, no. 1, pp. 311–324, Jan. 2019.

[11] K. Sun, Z. Qiu, H. Wu, and Y. Xing, "Evaluation on high-efficiency thermoelectric generation systems based on differential power processing," *IEEE Trans. Ind. Electron.*, vol. 65, no. 1, pp. 699–708, Jan. 2018.

[12] E. Candan, P. S. Shenoy, and R. C. N. Pilawa-Podgurski, "A series-stacked power delivery architecture with isolated differential power conversion for data centers," *IEEE Trans. Power Electron.*, vol. 31, no. 5, pp. 3690–3703, May 2016.

[13] G. Chu, H. Wen, Y. Hu, L. Jiang, Y. Yang, and Y. Wang, "Low-complexity power balancing point-based optimization for photovoltaic differential power processing," *IEEE Trans. Power Electron.*, vol. 35, no. 10, pp. 10306–10322, Oct. 2020.

[14] C. Olalla, D. Clement, M. Rodriguez, and D. Maksimovic, "Architectures and control of submodule integrated DC–DC converters for photovoltaic applications," *IEEE Trans. Power Electron.*, vol. 28, no. 6, pp. 2980–2997, Jun. 2013.

[15] C. Olalla, C. Deline, D. Clement, Y. Levron, M. Rodriguez, and D. Maksimovic, "Performance of power-limited differential power processing architectures in mismatched PV systems," *IEEE Trans. Power Electron.*, vol. 30, no. 2, pp. 618–631, Feb. 2015.

[16] M. Mao, C. Qian, and Y. Ding, "Decentralized coordination power control for islanding microgrid based on PV/BES-VSG," *CPSS Trans. Power Electron. Appl.*, vol. 3, no. 1, pp. 14–24, Mar. 2018.

[17] N. Liu, Q. Chen, X. Lu, J. Liu, and J. Zhang, "A charging strategy for PV-based battery switch stations considering service availability and self-consumption of PV energy," *IEEE Trans. Ind. Electron.*, vol. 62, no. 8, pp. 4878–4889, Aug. 2015.

[18] M. Tabari and A. Yazdani, "Stability of a dc distribution system for power system integration of plug-in hybrid electric vehicles," *IEEE Trans. Smart Grid*, vol. 5, no. 5, pp. 2564–2573, Sep. 2014.

[19] Q. Song, L. Wang, and J. Chen, "A decentralized energy management strategy for a fuel cell–battery hybrid electric vehicle based on composite control," *IEEE Trans. Ind. Electron.*, vol. 68, no. 7, pp. 5486–5496, Jul. 2021.

[20] Y. Pan, A. Sangwongwanich, Y. Yang, and F. Blaabjerg, "Distributed control of islanded series PV-battery-hybrid systems with low communication burden," *IEEE Trans. Power Electron.*, vol. 36, no. 9, pp. 10199–10213, Sep. 2021.

[21] B. Somaiah and V. Agarwal, "Distributed maximum power extraction from fuel cell stack arrays using dedicated power converters in series and parallel configuration," *IEEE Trans. Energy Convers.*, vol. 31, no. 4, pp. 1442–1451, Dec. 2016.

[22] N. Hou and Y. W. Li, "Overview and comparison of modulation and control strategies for a nonresonant single-phase dual-active-bridge DC–DC converter," *IEEE Trans. Power Electron.*, vol. 35, no. 3, pp. 3148–3172, Mar. 2020.

[23] F. An, W. Song, K. Yang, N. Hou, and J. Ma, "Improved dynamic performance of dual active bridge dc–dc converters using MPC scheme," *IET Power Electron.*, vol. 11, no. 11, pp. 1756–1765, 2018.

[24] W. Song, N. Hou, and M. Wu, "Virtual direct power control scheme of dual active bridge DC–DC converters for fast dynamic response," *IEEE Trans. Power Electron.*, vol. 33, no. 2, pp. 1750–1759, Feb. 2018.

[25] G. G. Oggier, M. Ordonez, J. M. Galvez, and F. Luchino, "Fast transient boundary control and steady-state operation of the dual active bridge converter using the natural switching surface," *IEEE Trans. Power Electron.*, vol. 29, no. 2, pp. 946–957, Feb. 2014.

[26] N. Vazquez and M. Liserre, "Peak current control and feed-forward compensation of a DAB converter," *IEEE Trans. Ind. Electron.*, vol. 67, no. 10, pp. 8381–8391, Oct. 2020.

[27] M. G. Villalva, J. R. Gazoli, and E. R. Filho, "Comprehensive approach to modeling and simulation of photovoltaic arrays," *IEEE Trans. Power Electron.*, vol. 24, no. 5, pp. 1198–1208, May 2009.

[28] H. A. Sher, A. F. Murtaza, A. Noman, K. E. Addoweesh, K. Al-Haddad, and M. Chiaberge, "A new sensorless hybrid MPPT algorithm based on fractional short-circuit current measurement and P&O MPPT," *IEEE Trans. Sustain. Energy*, vol. 6, no. 4, pp. 1426–1434, Oct. 2015.

[29] D. Zhou, A. Al-Durra, I. Matraji, A. Ravey, and F. Gao, "Online energy management strategy of fuel cell hybrid electric vehicles: A fractional-order extremum seeking method," *IEEE Trans. Ind. Electron.*, vol. 65, no. 8, pp. 6787–6799, Aug. 2018.

[30] N. Hou, L. Ding, P. Gunawardena, Y. Zhang, and Y. W. Li, "A comprehensive comparison of two fast-dynamic control structures for the DAB DC–DC converter," *IEEE Trans. Power Electron.*, vol. 37, no. 6, pp. 6488–6500, Jun. 2022.

[31] J. Hu, P. Joebges, G. C. Pasupuleti, N. R. Averous, and R. W. De Doncker, "A maximum-output-power-point-tracking-controlled dual-active bridge converter for photovoltaic energy integration into MVDC grids," *IEEE Trans. Energy Convers.*, vol. 34, no. 1, pp. 170–180, Mar. 2019.

[32] A. R. Amelia et al., "Investigation of the effect temperature on photovoltaic (PV) panel output performance," *Int. J. Adv. Sci. Eng. Inf. Technol.*, vol. 6, no. 5, pp. 682–688, 2016.

[33] S. Bhattacharyya, D. S. Kumar P, S. Samanta, and S. Mishra, "Steady output and fast tracking MPPT (SOFT-MPPT) for P&O and InC algorithms," *IEEE Trans. Sustain. Energy*, vol. 12, no. 1, pp. 293–302, Jan. 2021.

[34] M. A. G. de Brito, L. Galotto, L. P. Sampaio, G. d. A. e Melo, and C. A. Canesin, "Evaluation of the main MPPT techniques for photovoltaic applications," *IEEE Trans. Ind. Electron.*, vol. 60, no. 3, pp. 1156–1167, Mar. 2013.

[35] Q. Li et al., "Online extremum seeking-based optimized energy management strategy for hybrid electric tram considering fuel cell degradation," *Appl. Energy*, vol. 285, Mar. 2021, Art. no. 116505.

[36] T. Wang, Q. Li, Y. Qiu, L. Yin, L. Liu, and W. Chen, "Efficiency extreme point tracking strategy based on FFRLS online identification for PEMFC system," *IEEE Trans. Energy Convers.*, vol. 34, no. 2, pp. 952–963, Jun. 2019.

Nie Hou (Member, IEEE) received the B.Sc. and M.Sc. degrees from Southwest Jiaotong University, Chengdu, China, in 2014 and 2017, respectively, and the Ph.D. degree from University of Alberta, Edmonton, AB, Canada, in 2022, all in electrical engineering.

He is currently working as a Postdoctoral Fellow with the University of Alberta. His current research interests include digital control and optimization methods of dc–dc converters and dc distribution system.

Dr. Hou was the recipient of the Outstanding Author Award from the Proceeding of the Chinese Society for Electrical Engineering in 2016 and the second prize of IAS Sustainable and Renewable Energy Conversion System Committee Conference Paper Awards in 2021.

Li Ding (Member, IEEE) received the B.Sc. degree from Shanghai University, Shanghai, China, in 2013, the M.Sc. degree from Harbin Institute of Technology, Harbin, China, in 2015, and the Ph.D. degree from the University of Alberta, Edmonton, AB, Canada, in 2020, all in electrical engineering.

He is currently working as a Postdoctoral Fellow with the University of Alberta. His research interests include current-source converters, sensorless motor drives, multilevel converters, wide band-gap devices, and parameter identification.

Pasan Gunawardena (Graduate Student Member, IEEE) received the B.Sc. degree in electrical engineering and the M.Phil. degree in electronics and telecommunication engineering from the University of Moratuwa, Moratuwa, Sri Lanka, in 2015 and 2019, respectively. He is currently working toward the Ph.D. degree in the field of energy systems with the Department of Electrical and Computer Engineering, University of Alberta, Edmonton, AB, Canada.

His current research interests include dc–dc converter topologies and dc microgrid systems.

Mr. Gunawardena was the recipient of the second prize of the IAS Renewable and Sustainable Energy Conversion Systems Committee Conference Paper awards in 2021.

TianHong Wang (Member, IEEE) was born in Sichuan, China. He received the B.S. and Ph.D. degrees in electrical engineering from Southwest Jiaotong University, Chengdu, China, in 2016 and 2022, respectively. He is currently working toward the Ph.D. degree in electrical engineering from the University of Bourgogne FrancheComte, UTBM, Belfort, France.

His research interests include fuel cell modeling and optimal control, dc/dc converter control, energy management strategy of hybrid system, and fuel cell electrochemical impedance spectroscopy research.

Yue Zhang (Member, IEEE) received the B.Sc. and M.Sc. degrees from Nanjing University of Aeronautics and Astronautics, Nanjing, China, in 2012 and 2015, respectively, and the Ph.D. degree from Southeast University, Nanjing, China, in 2020, all in electrical engineering.

From 2017 to 2019, he was a Visiting Ph.D. student with the University of Alberta, Edmonton, AB, Canada, where he is currently a Postdoctoral Fellow. His research interests include dc/dc converters and magnetic design.

Yun Wei Li (Fellow, IEEE) received the B.Sc. degree in electrical engineering from Tianjin University, Tianjin, China, in 2002, and the Ph.D. degree in electrical engineering from Nanyang Technological University, Singapore, in 2006.

In 2005, he was a Visiting Scholar with Aalborg University, Denmark. From 2006 to 2007, he was a Postdoctoral Research Fellow with Ryerson University, Canada. In 2007, he also worked at Rockwell Automation Canada before he joined the University of Alberta, Edmonton, AB, Canada in the same year. Since 2007, he has been with the University of Alberta, where he is a Professor and Acting Department Chair currently. His research interests include distributed generation, microgrid, renewable energy, high power converters, and electric motor drives.

Dr. Li was the recipient of the Richard M. Bass Outstanding Young Power Electronics Engineer Award from IEEE Power Electronics Society in 2013. He serves as the Editor-in-Chief for IEEE TRANSACTIONS ON POWER ELECTRONICS LETTERS. Prior to that, he was an Associate Editor for IEEE TRANSACTIONS ON POWER ELECTRONICS, IEEE TRANSACTIONS ON INDUSTRIAL ELECTRONICS, IEEE TRANSACTIONS ON SMART GRID, and IEEE JOURNAL OF EMERGING AND SELECTED TOPICS IN POWER ELECTRONICS. He served as the general Chair of IEEE Energy Conversion Congress of Exposition (ECCE) in 2020. He is the AdCom Member at Large for IEEE Power Electronics Society (PELS) 2021–2023. He is recognized as a Highly Cited Researcher by the Web of Science Group.